

ON THE APPLICATION OF THE YIELD-LINE METHOD TO MASONRY INFILLS SUBJECTED TO COMBINED IN-PLANE AND OUT-OF-PLANE LOADS

Laura Liberatore¹, Omar AlShawa¹,

¹Department of Structural and Geotechnical Engineering, Sapienza University of Rome

Via Gramsci 53, 00197 Rome, Italy

{laura.liberatore,omar.alshawa}@uniroma1.it

Abstract. The influence of infills on the seismic response of frame structures has been long recognised. On the one hand, the presence of infills may be beneficial, due to their contribution to dissipate energy. On the other hand, irregular infill distributions in plan or elevation can lead to concentration of the displacement demand in localised parts of the building. It is noted that the lack of one or more panels may depend on the original building layout or may be generated by the infill collapse during a seismic event. It is therefore of interest the assessment of their capacity to resist out-of-plane loads.

In this paper, the use of the yield-line theory for the estimation of the out-of-plane infill strength is investigated. The method is described in detail and an example of derivation of the related equations is presented. Afterward, a modification of such equations is suggested to account for different contact conditions at the infill-frame interface. Moreover, specific attention is paid to the assessment of the masonry flexural strength, which is a basic parameter for the application of the method. Finally, a reduction factor is calibrated to extend the method to those cases in which previous in-plane damage is present. Experimental tests available in the literature are used to verify and calibrate the proposed equations and coefficients.

Keywords: *Infilled frame; Flexural strength; Out-of-plane collapse mechanism, Yield moment, Interstory drift ratio.*

1 INTRODUCTION

Reinforced concrete and steel framed structures are often infilled with unreinforced masonry walls. Generally, such walls are considered non-structural during the building design stage, even though their influence on the seismic response of buildings is widely recognized [1–6]. The extent of their effect depends on the relative stiffness and strength of the infill and the frame as well as on their distribution in plan and elevation [7]. To this concern, the collapse of an infill may cause adverse structural conditions, e.g. the development of irregular configurations, with consequent concentration of the displacement demand in localised parts of the building.

As observed after recent seismic events [8–12], the failure of infills, especially in the out-of-plane (OOP) direction, is frequent also in case of moderate earthquakes, causing a risk for life and socio-economic losses and the reduction of the structural capacity. This explains the increasingly growing efforts devoted to the study of the OOP response of infills and to the interaction between in-plane (IP) and OOP loads [13–21]. State of the art reviews may be found in [22,23]. One of the main goals of the published research is the assessment of the OOP strength, for which different approaches have been proposed, like those based on the one-way [24,25] or two-way [26,27] arching action. Such models are often calibrated and verified by means of experimental results [28–31]. Numerical methods, which resort to finite or discrete elements, have been used as well [32–34]. Other approaches are based on the yield-line theory, which was initially proposed to determine the collapse load of reinforced concrete slabs [35,36] and subsequently modified for use in the analysis of masonry walls [37,38]. The yield-line method consists in defining a kinematically compatible pattern (yield-line mechanism) and calculating the limit load by equating the internal and external works. It is assumed that the bending moment in a point of a yield line reaches the yield value and remains constant until such value is attained along the whole line. Clearly, this assumption cannot be achieved for a brittle material such as masonry and can lead to the overestimation of the limit load [39]. On the other hand, the method allows to take into account different strengths in two orthogonal directions and the bending resistance along supports [38]. In addition, even though actual yield-line behaviour cannot be theoretically justified, a substantial body of data demonstrates that the yield-line analyses provide quite good estimations, albeit slightly unconservative, of the failure pressure [40]. To obtain better predictions, some modifications were introduced, such as those included in the failure-line method and in the fracture-line method. In the former, the contribution of the first crack to the internal work is partially or totally disregarded [41,42], while a coefficient to take into account the stiffness orthotropy is introduced in the fracture-line method [43]. A comparison between yield-line, failure-line and fracture-line methods is presented in [44].

The yield-line and failure-line methods are probably the most adopted because they are implemented in codes in form of tabulated coefficients, thus simplifying their use. Specifically, the yield-line method was first introduced in the British Standard BS 5628 [45] and later on in Eurocode 6 [46], whereas the failure-line method was included in the Canadian Code [47]. On the other hand, the fracture-line method requires the knowledge of an additional parameter to take into account the stiffness orthotropy, thus entailing a further source of error.

The current approach implemented in codes applies to masonry walls rather than infills and assumes that the yield moments - when present - at the wall edges are the same as those at internal cracks. Obviously, the contact conditions that develop between an infill and the surrounding frame are different from those present in a masonry wall. In this study, to account for such feature, the yield-line equations are rewritten to allow the adoption of different yield moments at edges and along internal cracks. Moreover, a coefficient is introduced to take into account the vanishing of the yield moment at the first crack, as suggested in the failure-line method. Finally, an empirical factor is proposed to extend the method to those cases in which previous IP damage is present. Part of the study is devoted to the assessment and prediction of the masonry flexural strength, which is a basic parameter for the application of the method. To calibrate and validate the proposed equations and coefficients, two different datasets are employed: one including tests on wallettes subjected to bending, and the other one consisting of tests on one-bay one-storey infilled frames subjected to OOP or combined IP/OOP loads.

2 THE YIELD-LINE METHOD

The yield-line method consists in defining a kinematically compatible mechanism (yield-line mechanism) in which all deformations take place along yield lines and edges, and the single portions of the wall rotate as rigid bodies (Figure 1). The balance between external work and internal work, which is given by the energy dissipated along the yield lines, provides the value of the external load. Considering the upper bound theorem of the limit analyses, it is possible to recognise that the yield-line method provides an upper bound of the wall strength. Amongst the infinite number of mechanisms, the collapse mechanism is the one that occurs under the smallest load.

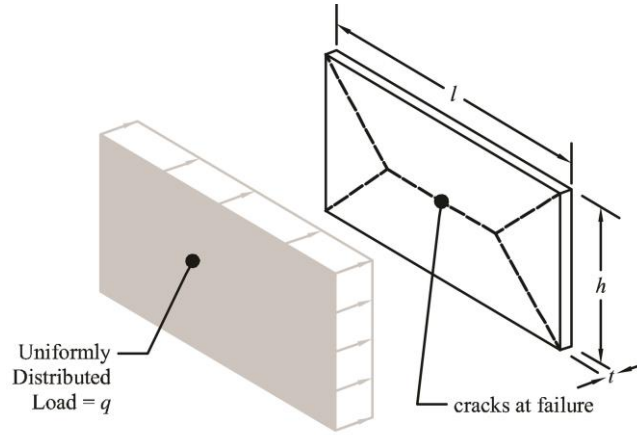


Figure 1: Kinematically compatible mechanism, each part of the panel rotates as a rigid body about the yield lines.

In the following subsection, the procedure to obtain the yield-line method equations is outlined for a panel bounded on four edges (§ 2.1), while in § 2.2 the equations are rewritten considering different yield moments at edges and along internal cracks and introducing a coefficient to take into account the vanishing of the yield moment at the first crack.

2.1 Yield-line equations

In the yield-line method the following assumptions are made:

- wall portions deflect as rigid bodies bordered by crack lines, the pattern of which defines a collapse mechanism (Figure 1);
- bending moment in a point of a yield line reaches the yield value (moment capacity) and remains constant until collapse; which is to say that moment capacities along all cracks are reached simultaneously at the point of ultimate strength [42];
- the flexural strength in the horizontal direction, f_{x1} , can be expressed as a function of the flexural strength in the vertical direction, f_{x2} :

$$f_{x1} = \mu f_{x2} \quad (1)$$

therefore,

$$m_1 = f_{x1} Z = \mu f_{x2} Z = \mu m_2 \quad (2)$$

where μ is the orthogonal ratio, m_1 and m_2 are yield moments in the horizontal and vertical directions, i.e. having the plane of failure parallel and normal to the bed joints, respectively (Figure 2); and Z is the elastic section modulus of unit height or unit length of the wall:

$$Z = t^2/6 \quad (3)$$

where t is the panel thickness.

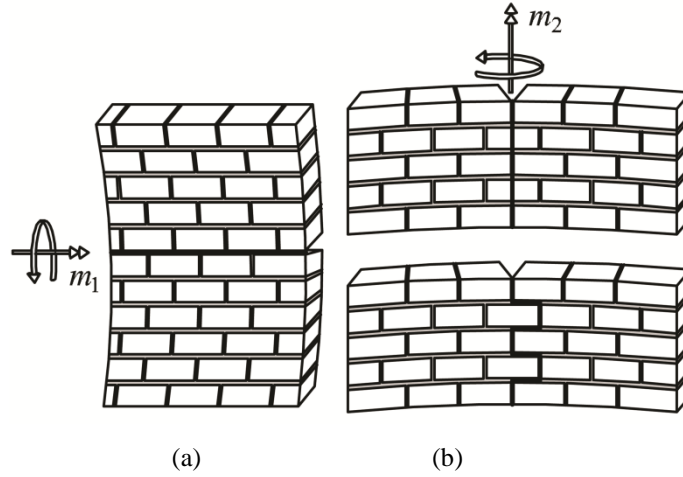


Figure 2: Plane of failure of masonry in bending: a) parallel to bed joints (flexural strength f_{x1} , yield moment m_1); b) perpendicular to bed joints (flexural strength f_{x2} , yield moment m_2).

Considering a wall fully restrained along four edges and loaded by a uniform pressure q , possible mechanisms are those represented in Figure 3.

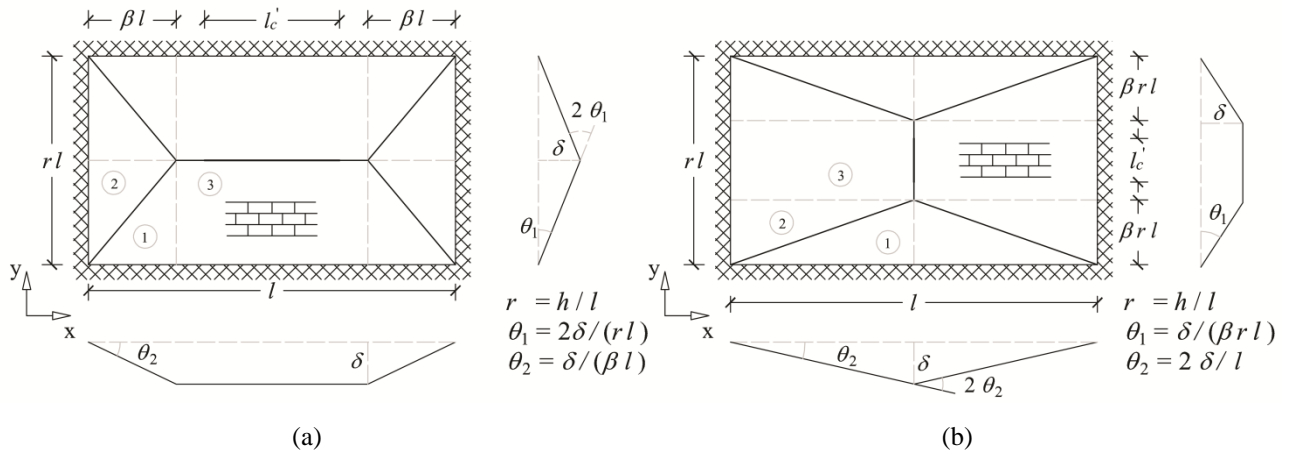


Figure 3: Possible collapse mechanisms of a wall fully restrained along four edges and loaded by a uniform pressure q .

For the mechanism in Figure 3a, dividing the wall area as shown in the figure, the work of external load is obtained by the sum of the following terms:

$$W_{ext,1} = \int_0^{\frac{rl}{2}} q \theta_1 y \left(\beta l - \frac{2\beta}{r} y \right) dy = \frac{1}{12} q \delta \beta r l^2 \quad (4)$$

$$W_{ext,2} = \int_0^{\beta l} q \theta_2 x \left(\frac{rl}{2} - \frac{r}{2\beta} x \right) dx = \frac{1}{12} q \delta \beta r l^2 \quad (5)$$

$$W_{ext,3} = \int_0^{\frac{rl}{2}} q \theta_1 y (l - 2\beta l) dy = \frac{1}{4} q \delta r l^2 (1 - 2\beta) \quad (6)$$

$$W_{ext} = 4W_{ext,1} + 4W_{ext,2} + 2W_{ext,3} = \frac{1}{6} q \delta r l^2 (3 - 2\beta) \quad (7)$$

The internal work is given by the sum of energies dissipated along the yield lines. Projecting the internal yield moments onto the horizontal and vertical axes, the internal work at internal cracks, $W_{int,1}$, and at the edges, $W_{int,2}$, are obtained:

$$W_{int,1} = m_1 2\theta_1 (l - 2\beta l) + 4 \left(m_1 \theta_1 \beta l + m_2 \theta_2 \frac{r l}{2} \right) = 4m_2 \delta \left(\frac{\mu}{r} + \frac{r}{2\beta} \right) \quad (8)$$

$$W_{int,2} = 2m_2 \theta_2 r l + 2m_1 \theta_1 l = 2m_2 \delta \left(\frac{r}{\beta} + \frac{2\mu}{r} \right) \quad (9)$$

Therefore, the total internal dissipated energy is:

$$W_{int} = W_{int,1} + W_{int,2} = 4m_2 \delta \left(\frac{2\mu}{r} + \frac{r}{\beta} \right) \quad (10)$$

Equating the external and internal works gives:

$$\frac{1}{6} q \delta r l^2 (3 - 2\beta) = 4m_2 \delta \left(\frac{2\mu}{r} + \frac{r}{\beta} \right) \quad (11)$$

$$q = \frac{24 m_2 (r^2 + 2\mu\beta)}{r^2 l^2 \beta (3 - 2\beta)} \quad (12)$$

The value of β is determined for minimum collapse load

$$\frac{\partial q}{\partial \beta} = 0 \quad (13)$$

which gives:

$$4\mu\beta^2 + 4r^2\beta - 3r^2 = 0 \quad (14)$$

Solving for β

$$\beta = \frac{-r^2 \pm \sqrt{r^4 + 3\mu r^2}}{2\mu} \leq 0.5 \quad (15)$$

Minimum collapse load is finally obtained by substituting the value of β into Eq. (12). Likewise, the following expressions of q of β are found for the mechanism in Figure 3b:

$$q = \frac{24m_2(2r^2\beta + \mu)}{r^2l^2\beta(3 - 2\beta)} \quad (16)$$

$$\beta = \frac{-\mu + \sqrt{3\mu r^2 + \mu^2}}{2r^2} \leq 0.5 \quad (17)$$

The collapse load is finally given by the minimum between Eq. (12) and Eq. (16).

As already mentioned, this method was implemented in codes in form of tabulated coefficients. For example, with reference to Eurocode 6 [46], the design moments per unit length in two orthogonal directions, M_{Ed1} and M_{Ed2} , applied to masonry walls subjected to a design lateral uniform pressure q_d can be calculated as:

$$M_{Ed1} = \alpha_1 q_d l^2 \quad (18)$$

$$M_{Ed2} = \alpha_2 q_d l^2 \quad (19)$$

where α_2 is a coefficient provided in Annex E [46] and $\alpha_1 = \mu \alpha_2$. Such moments must not be greater than the design values of the moment resistances m_{1d} and m_{2d}

$$\alpha_1 q_d l^2 \leq m_{1d} = f_{xd1} Z \quad (20)$$

$$\alpha_2 q_d l^2 \leq m_{2d} = f_{xd2} Z \quad (21)$$

Values of α_2 provided in Annex E are calculated through the yield-line theory as:

$$\alpha_2 = \frac{m_2}{q l^2} \quad (22)$$

where q is the uniform load which leads to collapse. For example, considering a wall fully restrained along four edges and under the hypothesis that minimum collapse load is given by Eq. (16), the coefficient α_2 is equal to:

$$\alpha_2 = \frac{r^2 l^2 \beta (3 - 2\beta)}{24(2r^2\beta + \mu) l^2} \quad (23)$$

2.2 Modified yield-line equations

In the procedure outlined above, it is implied that the yield moments m_1 and m_2 are the same at internal cracks and at cracks along the edges of the wall. This assumption is not adequate for an infill, especially along the vertical edges, where the bond between masonry and columns relies entirely on the head mortar joints along the contact surfaces. Therefore, to allow the adoption of different yield moments at the infill-frame interfaces (m_a and m_b in Figure 4), two coefficients (γ_a and γ_b) are introduced, so that:

$$m_a = \gamma_a m_1 = \gamma_a \mu m_2 = \gamma_a \mu f_{x2} Z \quad (24)$$

$$m_b = \gamma_b m_1 = \gamma_b f_{x1} Z \quad (25)$$

where m_a and m_b are the yield moments that develop at the vertical and horizontal edges, respectively, and γ_a and γ_b are coefficients that depend on the contact conditions between the masonry and the frame. Given that m_1 and m_2 are proportional to the masonry flexural strengths, γ_a and γ_b can be also regarded as factors applied to such strengths. Values assigned to γ_a and γ_b are specified in § 4.2 for different frame types.

To take into account the vanishing of the yield moment at the first crack, a reduction factor k is considered so that the length of the crack contributing to the internal work is:

$$l'_c = k l_c \quad (26)$$

for $k = 1$ the first crack is taken into account in the estimation of the internal work, while for $k = 0$ it is totally disregarded (like in the failure-line method).

With reference to the same example of the previous section (Figure 3), the internal work, given by the sum of energies dissipated along the internal yield lines, $W_{int,1}$, and at the edges, $W_{int,2}$, are:

$$\begin{aligned} W_{int,1} &= m_1 \Delta \theta_1 k (l - 2\beta l) + 4 \left(m_1 \theta_1 \beta l + m_2 \theta_2 \frac{rl}{2} \right) \\ &= 4m_2 \delta \left[\frac{\mu}{r} k (1 - 2\beta) + \frac{2\mu\beta}{r} + \frac{r}{2\beta} \right] \end{aligned} \quad (27)$$

$$W_{int,2} = 2m_a \theta_2 r l + 2m_b \theta_1 l = 2\mu m_2 \delta \left(\frac{\gamma_a r}{\beta} + \frac{2\gamma_b}{r} \right) \quad (28)$$

The total internal dissipated energy is given by:

$$W_{int} = W_{int,1} + W_{int,2} = 4m_2 \delta \left[\frac{\mu}{r} k (1 - 2\beta) + \frac{2\mu\beta}{r} + \frac{r}{2\beta} + \frac{\mu\gamma_a r}{2\beta} + \frac{\mu\gamma_b}{r} \right] \quad (29)$$

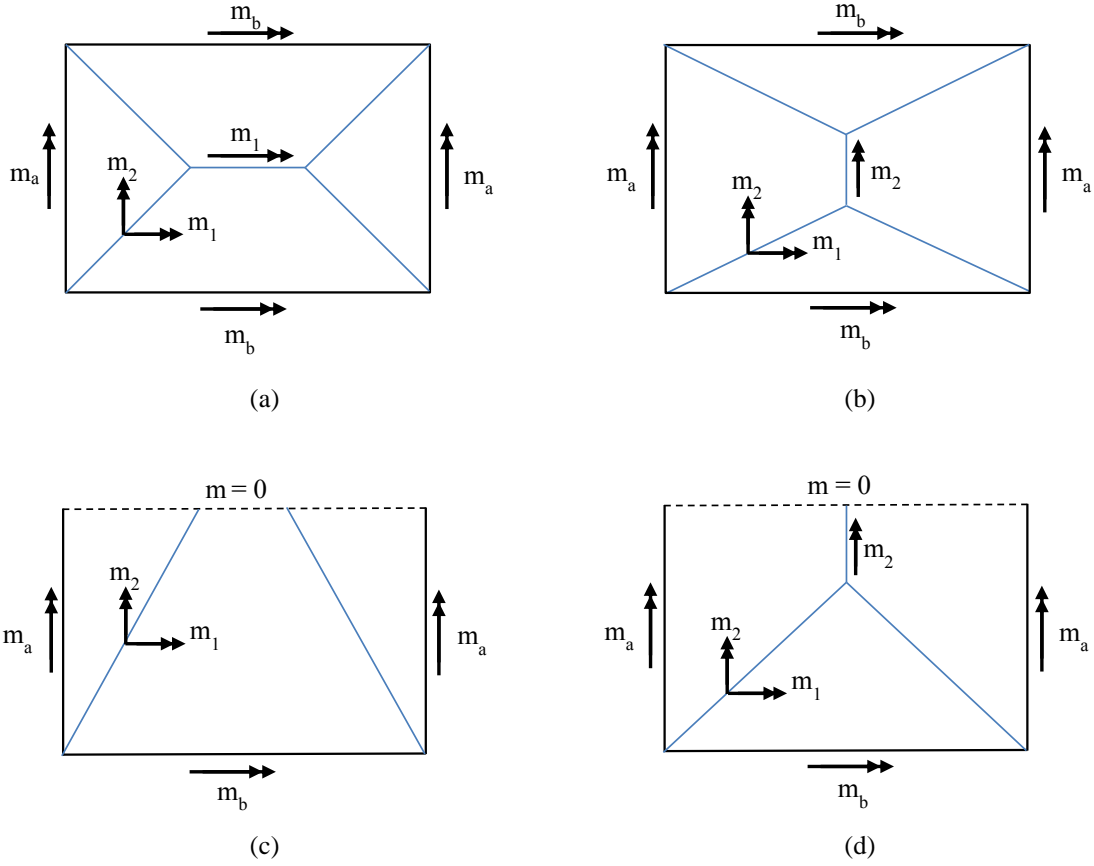


Figure 4: Yield-line pattern, under the assumption of rigid plate rotation within yield-line boundaries: a) and b) possible collapse mechanisms for a panel supported along four edges; c) and d) possible collapse mechanisms for a panel supported along three edges.

Equating the external work (Eq. (7)) to the internal one and finding the value of β related to the minimum collapse load gives:

$$\frac{1}{6}q\delta r l^2(3 - 2\beta) = 4m_2\delta \left[\frac{\mu}{r}k(1 - 2\beta) + \frac{2\mu\beta}{r} + \frac{r}{2\beta} + \frac{\mu\gamma_a r}{2\beta} + \frac{\mu\gamma_b}{r} \right] \quad (30)$$

$$q = 12m_2 \frac{4\mu(1 - k)\beta^2 + 2\mu(\gamma_b + k)\beta + (1 + \mu\gamma_a)r^2}{r^2 l^2 \beta(3 - 2\beta)} \quad (31)$$

$$\frac{\partial q}{\partial \beta} = 0 \quad (32)$$

$$(12\mu - 8k\mu + 4\gamma_b\mu)\beta^2 + (4r^2 + 4\gamma_a\mu r^2)\beta - 3r^2 - 3\gamma_a\mu r^2 = 0 \quad (33)$$

$$\beta = \frac{-(1 + \gamma_a\mu)r^2 + r\sqrt{(1 + \gamma_a\mu)(r^2 + 3(3 - 2k)\mu + r^2\gamma_a\mu + 3\gamma_b\mu)}}{2\mu(3 - 2k + \gamma_b)} \quad (34)$$

Minimum collapse load for mechanism in Figure 3a is then obtained by substituting the value of β into Eq. (31). In the same way, the following expressions of q and β are found for the mechanism in Figure 3b:

$$q = 12m_2 \frac{4r^2(1-k)\beta^2 + 2r^2(k + \gamma_a\mu)\beta + (1 + \gamma_b)\mu}{r^2l^2\beta(3 - 2\beta)} \quad (35)$$

$$\beta = \frac{-(1 + \gamma_b)\mu + \sqrt{(1 + \gamma_b)(3r^2\mu(3 - 2k) + \mu^2 + 3r^2\gamma_a\mu^2 + \gamma_b\mu^2)}}{2r^2(3 - 2k + \gamma_a\mu)} \quad (36)$$

Finally, the minimum between Eq. (31) and Eq. (35) gives the collapse pressure. With the same procedure, equations are found for different support conditions (Appendix A).

3 FLEXURAL STRENGTH AND ORTHOGONAL RATIO

The knowledge of the flexural strengths in two orthogonal directions or, which is the same, of the flexural strength in one direction and the orthogonal ratio, is a major requirement for the application of the yield-line method. These characteristics depend on a number of variables, such as the geometrical and mechanical characteristics of units, the mortar type and the thickness of mortar joints. An insight on solid clay brick masonry is given in [48], where the influence of the water absorption of the units and the use of additives to the mortar strength are specifically investigated. However, since the compressive strength of masonry is influenced by many of the factors which affect the flexural strength, a correlation between the two was suggested by Satti [49].

In this section, in order to find a relation between flexural and compressive strengths, a number of experimental tests carried out on masonry wallettes made of clay bricks or concrete blocks are investigated. A summary is reported in Table 1, whereas more details are given in a supplementary data file (*wallettes_experimental_tests* data sheet). The tests are performed on simply supported wallettes loaded along two lines as schematically reported in Figure 5a, or, less frequently, at midspan (Figure 5b).

The flexural strength in the direction normal to the bed joints (moment vector parallel to bed joints), normalised by the compressive strength is shown in Figure 6. The trend is somewhat sharp and highlights how the ratio f_{x1}/f_m decreases with increasing f_m . This outcome confirms that the normalised flexural strength, f_{x1}/f_m , can be expressed as a function of the compressive strength. Regression analysis provides the following equation:

$$f_{x1}/f_m = 0.154 f_m^{-0.902} \quad (37)$$

It is worth mentioning that the above formula is obtained from tests on simply supported specimens. The presence of frame elements, which hinder rotations at the edges and provide a confining action, enhances the infill flexural strength. Therefore, the use of Eq. (37) in the yield-line method is expected to provide conservative values of the OOP collapse load.

Reference	Flexural tests			Compressive tests ⁽¹⁾
	Number of tests	Code/standard	Lateral load	
Hendry (1973) [37] and Satti (1972) [49]	10	-	at centre	Unit and mortar
Hamid and Drysdale (1988) [50]	9	-	at two points	Unit and mortar
Angel <i>et al.</i> (1994) [25]	2	ASTM E518 ⁽²⁾	at two points	Prism tests
Brown and Melander (2001) [51]	8	ASTM C1390 ⁽³⁾	at two points	Unit and mortar
Varela-Rivera <i>et al.</i> (2011, 2012) [52,53]	3	ASTM E72 ⁽⁴⁾	at two points	Prism tests
Pereira <i>et al.</i> (2011, 2014) [54,55]	2	EN 1052-2 ⁽⁵⁾	at two points	Wallette tests
Singhal and Rai (2014) [56]	1	EN 1052-2 ⁽⁵⁾	at two points	Prism tests
Costigan and Pavia (2009) [57]	3	EN 1052-2 ⁽⁵⁾	at two points	Wallette tests
Raposo <i>et al.</i> (2018) [58]	1	EN 1052-2 ⁽⁵⁾	at two points	Unit and mortar
Anić <i>et al.</i> (2019) [59]	1	EN 1052-2 ⁽⁵⁾	at two points	Wallette tests
Furtado <i>et al.</i> (2020) [60]	4	EN 1052-2 ⁽⁵⁾	at two points	Wallette tests
Nalon <i>et al.</i> (2020) [61]	6	ASTM E518 ⁽²⁾	at two points	Prism tests

⁽¹⁾ Compressive strength is obtained either directly by experimental tests on masonry specimens (prisms or wallettes) or indirectly based on compressive tests on units and mortar.

⁽²⁾ ASTM E518, Standard test methods for flexural bond strength of masonry. ASTM International, West Conshohocken PA.

⁽³⁾ ASTM C1390-80, Test methods for flexural bond strength of masonry, ASTM International, West Conshohocken, PA.

⁽⁴⁾ ASTM E72, Standard test methods of conducting strength tests of panels for building construction. ASTM International, West Conshohocken, PA.

⁽⁵⁾ EN 1052-2, Methods of test for masonry - Part 2: Determination of flexural strength. London: British Standards Institution.

Table 1: Experimental tests on wallettes.

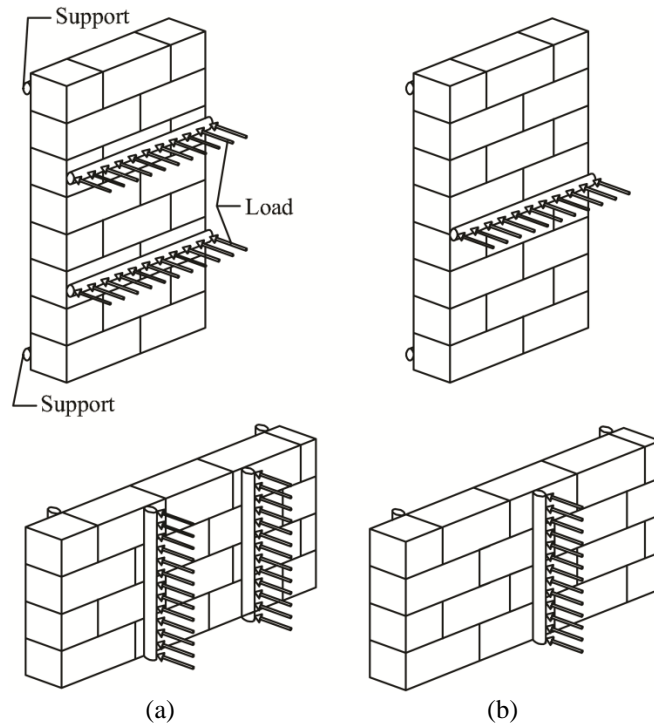


Figure 5: Flexural tests load patterns: a) along two lines; b) at midspan.

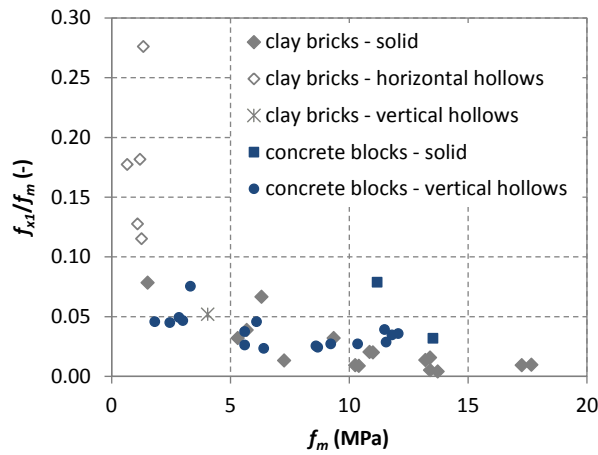


Figure 6: Flexural strength normal to the bed joints (moment vector parallel to bed joints), normalised by the compressive strength. Values are obtained from experimental tests on wallettes (Table 1).

The orthogonal ratio, i.e. the ratio between the flexural strengths normal and parallel to bed joints, f_{x1}/f_{x2} , shows different trends depending on whether the masonry is made of clay bricks or concrete blocks. In the former case, the orthogonal ratio decreases with increasing compressive strength (Figure 7a), whereas in the latter case a clear tendency is not present (Figure 7b). In conclusion, the following equations of the orthogonal ratio are proposed for clay brick masonry and for concrete block masonry, respectively:

$$\mu = f_{x1}/f_{x2} = 0.539 f_m^{-0.463} \quad (38)$$

$$\mu = f_{x1}/f_{x2} = 0.39 \quad (39)$$

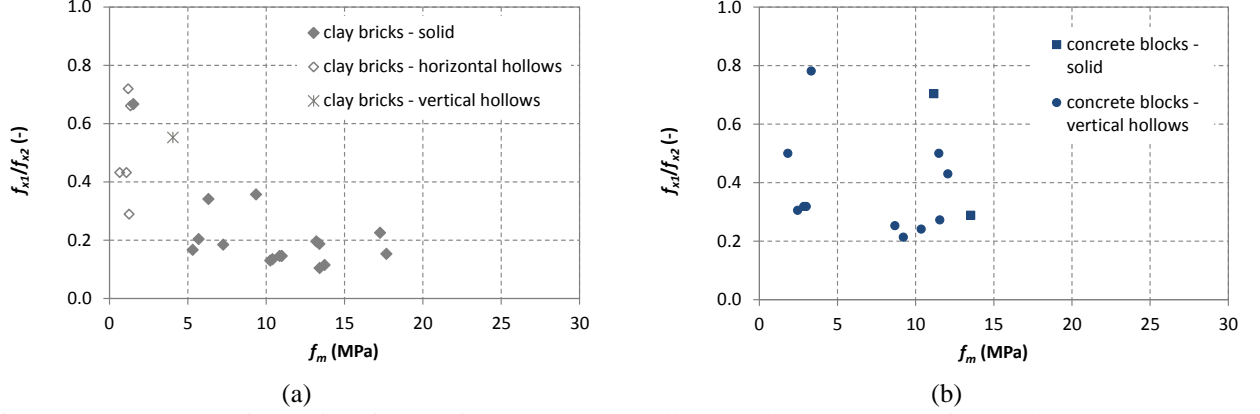


Figure 7: Orthogonal ratio obtained in experimental tests on wallettes (Table 1): a) clay bricks wallettes; b) concrete blocks wallettes.

The errors related to the use of Eq. (37), (38) and (39), estimated through the logarithmic standard deviation, σ_{ln} , of the ratio between predicted and experimental values, are 0.49, 0.37 and 0.40, respectively.

4 CALIBRATION OF THE MODIFIED YIELD-LINE METHOD

As mentioned above, equations presented in Appendix A require the knowledge of the masonry strength in bending. A first attempt to estimate this parameter is described in § 3. However, in experimental tests on wallettes the flexural strength is evaluated on simply supported specimens (Figure 5), thus a conservative estimate of the OOP collapse load is expected when using such results. For this reason, a dataset of experimental tests on infilled frames is also employed to calibrate a better equation of the flexural strength for use in the yield-line method. Subsequently, the effect of prior IP damage is introduced by modifying the parameters γ_a , γ_b and k .

4.1 Experimental dataset

A database consisting of 191 experimental tests on infilled frames was compiled in a previous research [21]. In the present study, tests without a surrounding frame as well as those in which infill walls were reinforced or strengthened or were not engaged until failure were disregarded (125 tests), while 6 more recent tests were added. Hence, the final experimental dataset includes 72 tests (Table

2 and *infills_experimental_tests* data sheet of the supplementary file), 39 of which are pure OOP, whereas 33 specimens were previously subjected to prior IP damage. The first group is used to assess the horizontal flexural strength. The second bunch is used to calibrate the parameters to take into account the IP-OOP interaction.

In the experimental tests, frames are mostly made of reinforced concrete (59 samples), whereas in 13 cases they are steel frames. Tests on confined masonry are considered as well (12 out of 59). They differ from infilled frames for the construction sequence. In fact, in infilled frames the infill is constructed after the frame, while in the case of confined masonry the wall is built before the frame, and RC beam and columns are subsequently cast against the masonry. As a consequence, a stronger bond develops between the two materials, especially at the vertical edges, where a toothed connection is often present [62]. These different conditions are taken into account in the application of the yield line method by adopting a different value for the coefficient γ_a , as explained in § 4.2.

Aspect and slenderness ratios are representative of typical infilled frames. The former value is in the range 0.5-1.0 (Figure 8a), with the majority (64%) having an aspect ratio between 0.6 and 0.8, the latter is not greater than 25 in 95% of the cases (Figure 8b).

In 46 tests the walls were made up of clay bricks having horizontal or vertical hollows or solid bricks, whereas concrete blocks having vertical hollows were used in 26 specimens. The masonry compressive strength varies between 0.5 and 30.5 MPa (Figure 8c), but in 80% of the cases it not greater than 15.0 MPa. Higher values are related to concrete block infills.

In 39 tests the infills were loaded in the OOP direction only. Generally, the OOP loads were applied monotonically by means of airbags, in some cases they were applied at four points or at mid-height. In the latter cases the equivalent uniform pressure was estimated so as to provide the same maximum bending moment as the concentrated forces. Some remarks on this aspect are given in § 4.3. Finally, the interaction between IP and OOP actions was considered in 33 tests, where an IP horizontal displacement was applied at the beam level prior to the OOP load.

Experimental results are generally presented in terms of force-displacement curves. Often, the qualitative behaviour is also described. By a comparison between different experimental campaigns it appears that establishing a clear correspondence between collapse mechanisms and geometrical and mechanical characteristics of the infill and the frame is not straightforward. However, for rectangular infills bounded along four edges the most frequent mechanism is that shown in Figure A2a (Appendix A), whereas specimens having an infill-beam gap showed crack patterns similar to those in Figure A2d. Nevertheless, in some cases the latter mechanism was observed also in infills with no gap, thus indicating the weakness of the infill-upper beam bond with respect to those along

the other edges. Finally, in some experimental tests the infill presented also smeared cracks. This occurred especially for infills made of clay bricks with horizontal hollows, while solid clay bricks and concrete blocks with vertical hollows showed sharper crack patterns.

Reference	OOP ⁽¹⁾	IP-OOP ⁽²⁾	Frame ⁽³⁾	Masonry units	Boundary conditions ⁽⁴⁾	OOP load type
Dawe and Seah (1989) [26]	6	-	Steel	Vertical hollow concrete blocks	3 edges (1) 4 edges (5)	airbag
Angel <i>et al.</i> (1994) [25]	1	5	RC	Solid clay bricks	4 edges	airbag
Flanagan (1994) [28]						
Flanagan and Bennett (1999) [63]	3	3	Steel	Horizontal hollow clay bricks	4 edges	airbag
Calvi and Bolognini (2001) [64]	1	2	RC	Horizontal hollow clay bricks	4 edges	loaded at four points
Pereira <i>et al.</i> (2011, 2014) [54,55]	-	4	RC	Horizontal hollow clay bricks	4 edges	airbag
Varela-Rivera <i>et al.</i> (2011) [52]	6	-	CM	Vertical hollow concrete blocks	3 edges (3) 4 edges (3)	airbag
Varela-Rivera <i>et al.</i> (2012) [53]	6	-	CM	Vertical hollow concrete blocks	4 edges	airbag
Da Porto <i>et al.</i> (2013) [65]	-	3	RC	Horizontal (1) and vertical (2) hollow clay bricks	4 edges	loaded at four points
Hak <i>et al.</i> (2014) [66]						
and Morandi <i>et al.</i> (2018) [67]	-	3	RC	Vertical hollow clay bricks	4 edges	loaded at mid-height
Furtado <i>et al.</i> (2016) [68]	2	1	RC	Horizontal hollow clay bricks	4 edges	airbag
Akhoundi <i>et al.</i> (2016) [69]	1	-	RC	Horizontal hollow clay bricks	4 edges	airbag
Wang (2017) [70]	3	1	RC (3) Steel (1)	Vertical hollow concrete blocks	3 edges (1) 4 edges (3)	airbag
Sepasdar (2017) [71]	2	2	RC	Vertical hollow concrete blocks	4 edges	airbag
Ricci <i>et al.</i> (2018) [72]	1	3	RC	Horizontal hollow clay bricks	4 edges	loaded at four points
De Risi <i>et al.</i> (2019) [73]	1	3	RC	Horizontal hollow clay bricks	4 edges	loaded at four points
Di Domenico <i>et al.</i> (2019) [74]	3	-	RC	Horizontal hollow clay bricks	3 edges (2) 4 edges (1)	loaded at four points
Akhoundi <i>et al.</i> (2020) [75]	3	3	RC	Horizontal hollow clay bricks	4 edges	airbag

⁽¹⁾ number of tests subjected to OOP loads only; ⁽²⁾ number of tests subjected to IP displacement and OOP load; ⁽³⁾ RC = Reinforced Concrete, CM = Confined Masonry; ⁽⁴⁾ Number of restrained edges.

Table 2: Experimental tests on infilled frames.

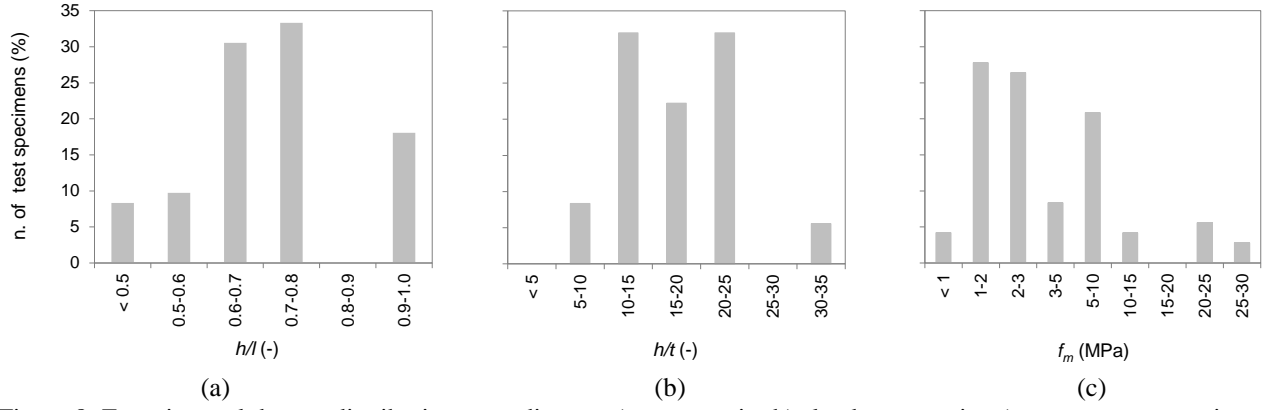


Figure 8: Experimental dataset distribution according to: a) aspect ratio; b) slenderness ratio; c) masonry compressive strength.

4.2 Model calibration

First and foremost, modified yield-line equations and pure OOP experimental tests are used to calibrate prediction equations of the horizontal flexural strength f_{x1} . Based on Eq. (2), experimental values of f_{x1} are obtained as:

$$f_{x1,exp} = \frac{\mu m_{2,exp}}{Z} \quad (40)$$

where $m_{2,exp}$ is the yield moment corresponding to the experimental collapse pressure and it is found from yield-line equations in Appendix A. The equation parameters, i.e. μ , γ_a , γ_b and k , are assumed as follows.

- If experimental values are not available, the orthogonal ratio, μ , is estimated by means of Eq. (38) for clay brick masonry and Eq. (39) for concrete block masonry.
- γ_a , and γ_b are considered constant in case of pure OOP loads and equal to the values reported in Table 3. In RC frames the flexural strength at the infill-frame interfaces (both horizontal and vertical) is assumed equal to the horizontal flexural strength of the masonry (Figure 2a), thus assuming that the mortar-concrete bond is the same as the horizontal mortar-brick bond. In case of confined masonry, given the stronger masonry-columns bond, the vertical flexural strength at edges is assumed equal to the vertical flexural strength of masonry, thus $\gamma_a = 1/\mu$. Finally, for steel frames the infill-frame bond is disregarded ($\gamma_a = \gamma_b = 0$).
- k is assumed equal to 1 in case of pure OOP loads, this means that the contribution of the first crack to the internal work is taken into account, consistently with the yield-line method.

All the values are summarised in Table 3.

	μ		γ_a	γ_b	k
	clay brick Eq. (38)	concrete block Eq. (39)			
RC frames			1	1	1
Confined masonry	$0.539 f_m^{-0.463}$ ⁽¹⁾	0.39 ⁽¹⁾	$1/\mu$	1	1
Steel frames			0	0	1

⁽¹⁾ unless experimental values are available

Table 3: Equation parameters for pure OOP loads.

Once the horizontal flexural strength ($f_{x1,exp}$) is found, a prediction equation able to correlate such parameter to the compressive strength is sought. Specifically, based on experimental values of the ratio $f_{x1,exp}/f_{m,exp}$ and taking advantage of the results reported in § 3, i.e. that such ratio can be expressed by means of a power function, the following equation is proposed:

$$f_{x1}/f_m = 0.35 f_m^{-0.745} \quad (41)$$

where the coefficients are obtained through a regression analysis. Experimental values, Eq. (37) and Eq. (41) are compared in Figure 9, whereas OOP strength predictions using Eq. (37) and Eq. (41) are shown in Figure 10a and Figure 10b, respectively. As expected, the experimental OOP collapse load is underestimated when using Eq. (37), being the exponential of the logarithmic mean, $e^{\mu_{ln}}$, and the logarithmic standard deviation, σ_{ln} , of the ratio between predicted and experimental strength equal to 0.36 and 0.34. In contrast, Eq. (41) is suitable for use in the modified yield line method, consistently with the way in which it was derived. In fact, it provides values of the OOP strength well matched with the experimental ones (Figure 10b). In this case, $e^{\mu_{ln}}$ and σ_{ln} are equal to 1.00 and 0.30, respectively.

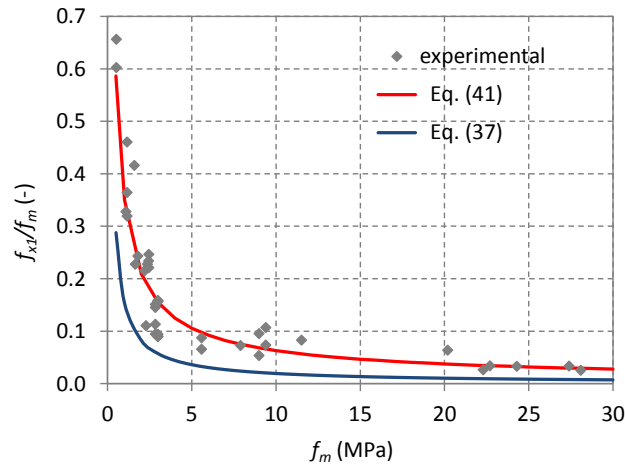


Figure 9: Normalised horizontal flexural strength: experimental and predicted values

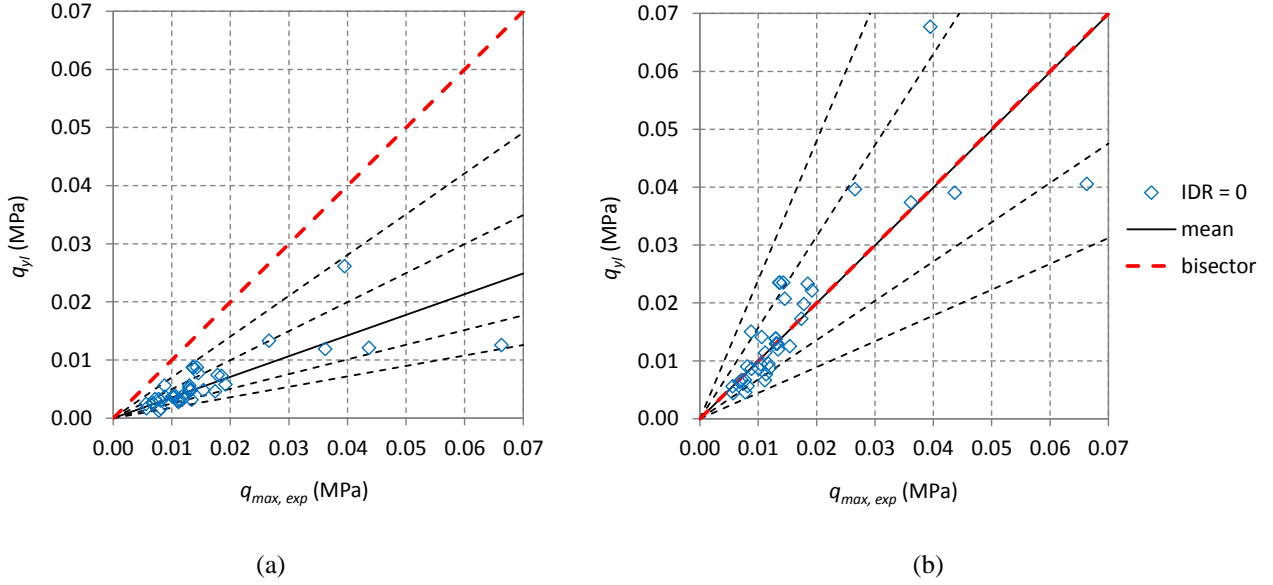


Figure 10: OOP strength of infill in pure OOP tests: predictions vs. experimental values. Values obtained using Eq. (37) (a) and Eq. (41) (b) for the estimation of the masonry horizontal flexural strength. Black dotted lines represent the mean \pm one and two standard deviations.

As mentioned above, the presence of cracks due to prior IP damage may reduce the OOP strength. To take into account this circumstance, the following assumptions are made:

- 1) the first crack (horizontal or vertical depending on the collapse mechanism) does not contribute to the total resistance when previous IP damage is present; therefore, the coefficient k is assumed equal to 0;
- 2) the moment contribution at the infill edges decreases due to the detachment between the infill and the frame associated to the IP drift, which causes a sliding at the horizontal edges and a partial detachment along the vertical edges;
- 3) the decrease of the yield moment at edges is function of the interstory drift ratio IDR .

Based on these premises, the effect IP damage is taken into account by reducing the yield moments m_a and m_b . This reduction is accomplished by modifying the coefficients γ_a and γ_b (Eq. (24) (25)) through a reduction factor, R_{IP} .

$$\gamma_{a,IP} = R_{IP} \gamma_a \quad (42)$$

$$\gamma_{b,IP} = R_{IP} \gamma_b \quad (43)$$

A regression analysis is performed in order to find an adequate expression of R_{IP} . More precisely, considering the experimental tests subjected to previous IP damage ($IDR \neq 0$), a reduction factor able to provide a good match between experimental and predicted OOP strength is determined so

that the exponential of the logarithmic mean, $e^{\mu_{ln}}$, of the ratio between predicted and experimental values is close to 1.0. The following expression is finally proposed:

$$R_{IP} = \min\left(\frac{0.02}{IDR^2}, 1\right) \quad (44)$$

Clearly, the reduction factor is always less than 1 and decreases with increasing IDR . The comparison between the OOP strength predicted by the proposed model and the experimental strength is presented in Figure 11, considering both infills loaded only OOP and infills with previous IP damage. Values of $e^{\mu_{ln}}$ and the corresponding logarithmic standard deviation, σ_{ln} , are reported in Table 4 for different ranges of IDR .

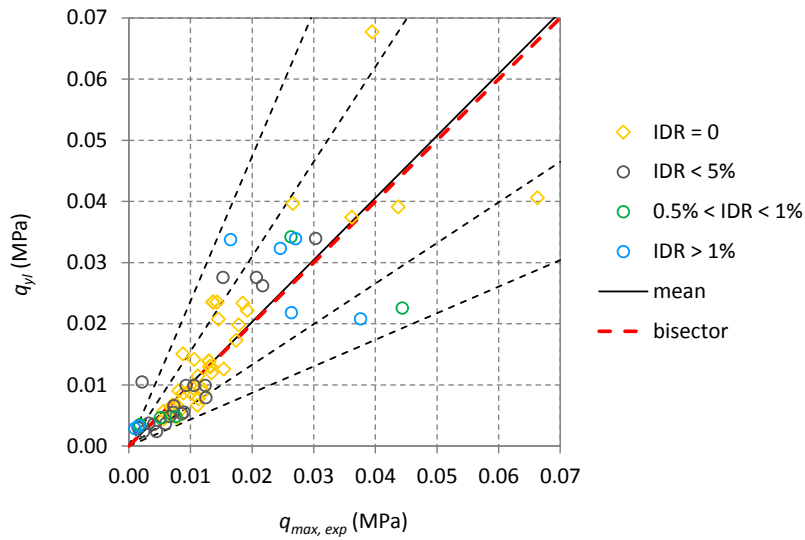


Figure 11: OOP strength of infill: predictions vs. experimental values. Black dotted lines represent the mean \pm one and two standard deviations.

	$e^{\mu_{ln}}$	σ_{ln}
OOP only ($IDR = 0.0\%$)	1.00	0.30
IP+OOP (all drift)	1.08	0.53
IP+OOP ($0.0\% < IDR \leq 0.5\%$)	1.03	0.51
IP+OOP ($0.5\% < IDR \leq 1.0\%$)	0.93	0.48
IP+OOP ($IDR > 1.0\%$)	1.37	0.53
Whole database	1.03	0.42

Table 4: Exponential of the logarithmic mean, $e^{\mu_{ln}}$, and logarithmic standard deviation, σ_{ln} , of the ratio between predicted and experimental values of the OOP strength.

Better predictions are obtained when there is no previous IP damage ($IDR = 0$), being $e^{\mu_{ln}}$ equal to 1.00, while in case of IDR greater than 1.0% the model overestimates the strength ($e^{\mu_{ln}}$ equal to 1.37). Concerning the standard deviation, it is possible to observe that it is smaller when no previous IP damage is present and greater in the opposite case, indicating that the IP damage results in a higher scatter. This is due to the fact that, when the infill is severely damaged with distributed cracks and crushed portions, the actual behaviour cannot be fully represented by a yield line mechanism. It is worth mentioning that other studies recommend to disregard the OOP strength when the IDR is equal to or greater than 1.0 % [76] or to reduce it to less than 20% of the OOP strength obtained in case of no previous IP damage [72].

4.3 Additional remarks

The calibration of both equations Eq. (41) and Eq. (44) was carried out considering the dataset in Table 2, which includes tests performed with airbags as well as tests in which the OOP load was applied in four points or at mid-height (20 test out of 72). In the latter cases, an equivalent uniform pressure giving the same maximum bending moment as the concentrated forces was considered. To evaluate the extent of the error generated from this simplification and verify the validity of the proposed equations, an additional comparison was carried out considering only the tests in which the OOP load was applied uniformly. Such comparison is reported in Table 5. Contrarily to what presented in Table 4, different ranges of IDR are not considered because the number of tests with previous IP damage in each range is inadequate for statistical assessments when the tests with OOP concentrated loads are disregarded.

With reference to Table 5, the results obtained using the whole database and those obtained with the “reduced” database are very close to one another when considering the pure OOP tests. A greater difference is observed in the IP+OOP tests. However, such difference is on the conservative side. In

fact, considering the cases in which an uniform pressure was applied, the predicted average strength is lower than the experimental one ($\sigma_{ln} = 0.96$).

	All specimens		Specimens loaded by uniform pressure	
	$e^{\mu_{ln}}$	σ_{ln}	$e^{\mu_{ln}}$	σ_{ln}
OOP only	1.00	0.30	1.02	0.32
IP+OOP (all drift)	1.08	0.53	0.96	0.53
Whole database	1.03	0.42	1.00	0.43

Table 5: Exponential of the logarithmic mean, $e^{\mu_{ln}}$, and logarithmic standard deviation, σ_{ln} , of the ratio between predicted and experimental values of the OOP strength.

5 CONCLUSIONS

This study is focused on the assessment of the OOP strength of masonry infills through the yield-line method. The method is based on the definition of kinematically compatible mechanisms and on the balance between external work and internal work. The main issues related with its employment are:

- the assessment of the masonry flexural strengths in two orthogonal directions, which are required to calculate the yield moments;
- the definition of the contact conditions between the infill and the surrounding frame;
- the need to include the IP damage effect in the evaluation of the OOP strength.

Concerning the first point, it is observed that the flexural strength is a parameter rarely estimated for infills, which are not designed to resist vertical or horizontal loads. For this reason, an attempt was made to correlate the flexural strength to the masonry compressive strength. Initially, experimental tests on wallettes were considered, but due to the fact that such tests were carried out on specimens under simple support conditions, an underestimation of the strength was observed. This suggested resort to OOP experimental tests on infilled frames, which brought to Eq. (41).

The second and third aspects were solved by introducing two coefficients, γ_a and γ_b , to express the yield moments at the infill-frame interfaces as functions of the yield moment of masonry in the horizontal direction. The factor k (Eq. (26)) was also introduced to control the contribution of the first crack to the internal work. The modified yield line equations were obtained (Appendix A) and experimental tests on infilled frames used to calibrate the model coefficients. In the proposed model, the presence of previous IP damage is taken into account by a reduction factor, R_{IP} , which depends on the IDR and is applied to γ_a and γ_b , i.e. to the yield moments at the infill-frame contact.

However, for *IDR* greater than 1%, the model overestimates, on the average, the strength, while for smaller *IDR* it is adequate to reproduce the strength provided the values reported in Table 3 and Eq. (41) to (43) are used for the involved parameters.

In conclusion, the equations reported in Appendix A are proposed to extend the yield-line method, already adopted for masonry walls, to infills subjected to OOP lateral loads. Such equations provide their OOP strength, to be used in local assessments of infills in both new and existing buildings. By using the proposed formulas, different situations can be considered, for example the presence of a top or lateral gap or the occurrence of a weaker or stronger infill-frame bond. In addition, the presence of previous IP damage can be accounted for through the factors k and R_{IP} . Finally, it is worth mentioning that, even though the method stems from a mechanical approach, experimental data were used to calibrate the involved coefficients empirically.

ACKNOWLEDGEMENTS

This work has been carried out under the program “Dipartimento di Protezione Civile – Consorzio RELUIS”. The opinions expressed in this publication are those of the authors and are not necessarily endorsed by the Dipartimento della Protezione Civile.

REFERENCES

- [1] Dolšek M, Fajfar P. The effect of masonry infills on the seismic response of a four storey reinforced concrete frame-a probabilistic assessment. *Eng Struct* 2008;30:3186–92. doi:10.1016/j.engstruct.2008.04.031.
- [2] Tanganelli M, Viti S, de Stefano M, Reinhorn AM. Influence of infill panels on the seismic response of existing RC buildings: A case study. *Geotech Geol Earthq Eng* 2013;24:119–33. doi:10.1007/978-94-007-5377-8__9.
- [3] De Luca F, Verderame GM, Gómez-Martínez F, Pérez-García A. The structural role played by masonry infills on RC building performances after the 2011 Lorca, Spain, earthquake. *Bull Earthq Eng* 2014;12:1999–2026. doi:10.1007/s10518-013-9500-1.
- [4] Liberatore L, Mollaioli F. Influence of Masonry Infill Modelling on the Seismic Response of Reinforced Concrete Frames. *Proc. Fifteenth Int. Conf. Civil, Struct. Environ. Eng. Comput.*, 2015. doi:10.4203/ccp.108.87.
- [5] Liberatore L, Noto F, Mollaioli F, Franchin P. Comparative assessment of strut models for

- the modelling of in-plane seismic response of infill walls. *COMPADYN 2017, 6th Int. Conf. Comput. Methods Struct. Dyn. Earthq. Eng.*, 2017. doi:10.7712/120117.5643.17476.
- [6] Liberatore L, Noto F, Mollaioli F, Franchin P. In-plane response of masonry infill walls: Comprehensive experimentally-based equivalent strut model for deterministic and probabilistic analysis. *Eng Struct* 2018;167:533–48. doi:10.1016/j.engstruct.2018.04.057.
- [7] Liberatore L, Decanini LD. Effect of infills on the seismic response of high-rise RC buildings designed as bare according to Eurocode 8. *Ing Sismica* 2011;28:7–23.
- [8] Braga F, Manfredi V, Masi A, Salvatori A, Vona M. Performance of non-structural elements in RC buildings during the L’Aquila, 2009 earthquake. *Bull Earthq Eng* 2011;9:307–24. doi:10.1007/s10518-010-9205-7.
- [9] Decanini LD, Liberatore L, Mollaioli F. Damage potential of the 2009 L’Aquila, Italy, earthquake. *J Earthq Tsunami* 2012;06:1250032. doi:10.1142/S1793431112500327.
- [10] Inel M, Ozmen HB, Akyol E. Observations on the building damages after 19 May 2011 Simav (Turkey) earthquake. *Bull Earthq Eng* 2013;11:255–83. doi:10.1007/s10518-012-9414-3.
- [11] Masi A, Chiauzzi L, Santarsiero G, Manfredi V, Biondi S, Spacone E, et al. Seismic response of RC buildings during the Mw 6.0 August 24, 2016 Central Italy earthquake: the Amatrice case study. *Bull Earthq Eng* 2017;1–24. doi:10.1007/s10518-017-0277-5.
- [12] Mazza F, Donnici A. In-plane and out-of-plane seismic damage of masonry infills in existing r.c. structures: the case study of De Gasperi-Battaglia school in Norcia. *Bull Earthq Eng* 2020. doi:10.1007/s10518-020-00981-2.
- [13] Komaraneni S, Rai DC, Singhal V. Seismic behavior of framed masonry panels with prior damage when subjected to out-of-plane loading. *Earthq Spectra* 2011;27:1077–103. doi:10.1193/1.3651624.
- [14] Mosalam KM, Günay S. Progressive collapse analysis of reinforced concrete frames with unreinforced masonry infill walls considering in-plane/out-of-plane interaction. *Earthq Spectra* 2015;31:921–43. doi:10.1193/062113EQS165M.
- [15] Walsh KQ, Dizhur DY, Shafaei J, Derakhshan H, Ingham JM. In Situ Out-of-Plane Testing of Unreinforced Masonry Cavity Walls in as-Built and Improved Conditions. *Structures* 2015;3:187–99. doi:10.1016/j.istruc.2015.04.005.
- [16] Liberatore L, Pasca M. Assessment of the Out-of-Plane Resistance of Masonry Infill Walls. *Proc. Fifteenth Int. Conf. Civil, Struct. Environ. Eng. Comput.*, 2015. doi:10.4203/ccp.108.173.

- [17] Tomassetti U, Graziotti F, Penna A, Magenes G. Modelling one-way out-of-plane response of single-leaf and cavity walls. *Eng Struct* 2018;167:241–55. doi:10.1016/j.engstruct.2018.04.007.
- [18] Dizhur D, Walsh K, Giongo I, Derakhshan H, Ingham J. Out-of-plane Proof Testing of Masonry Infill Walls. *Structures* 2018;15:244–58. doi:10.1016/j.istruc.2018.07.003.
- [19] Vaculik J, Griffith MC. Out-of-plane shaketable testing of unreinforced masonry walls in two-way bending. *Bull Earthq Eng* 2018;16:2839–76. doi:10.1007/s10518-017-0282-8.
- [20] Mazza F. In-plane–out-of-plane non-linear model of masonry infills in the seismic analysis of r.c.-framed buildings. *Earthq Eng Struct Dyn* 2019;48. doi:10.1002/eqe.3143.
- [21] Liberatore L, AlShawa O, Marson C, Pasca M, Sorrentino L. Out-of-plane capacity equations for masonry infill walls accounting for openings and boundary conditions. *Eng Struct* 2020. doi:10.1016/j.engstruct.2020.110198.
- [22] Asteris PG, Cavaleri L, Di Trapani F, Tsaris AK. Numerical modelling of out-of-plane response of infilled frames: State of the art and future challenges for the equivalent strut macromodels. *Eng Struct* 2017;132:110–22. doi:10.1016/j.engstruct.2016.10.012.
- [23] Pasca M, Liberatore L, Masiani R. Reliability of analytical models for the prediction of out-of-plane capacity of masonry infills. *Struct Eng Mech* 2017;64:765–81. doi:10.12989/sem.2017.64.6.765.
- [24] McDowell EL, McKee KE, Sevin E. Arching theory of masonry walls. *J Struct Div* 1956;82:915–1–915–8.
- [25] Angel R, Abrams D, Shapiro D, Uzarski J, Webster M. Behavior of Reinforced Concrete Frames with Masonry Infills, University of Illinois Engineering Experiment Station. College of Engineering. University of Illinois at Urbana-Champaign. ISSN: 0069-4274. vol. SRS-589. 1994.
- [26] Dawe JL, Seah CK. Out-of-plane resistance of concrete masonry infilled panels. *Can J Civ Eng* 1989;16:854–64. doi:10.1139/189-128.
- [27] Bashandy T, Rubiano N, Klingner R. Evaluation and Analytical Verification of Infilled Frame Test Data. 1995.
- [28] Flanagan RD. Behavior of structural clay tile infilled frames. University of Tennessee, Knoxville, 1994.
- [29] Ricci P, Di Domenico M, Verderame GM. Experimental investigation of the influence of slenderness ratio and of the in-plane/out-of-plane interaction on the out-of-plane strength of URM infill walls. *Constr Build Mater* 2018. doi:10.1016/j.conbuildmat.2018.10.011.

- [30] Di Domenico M, Ricci P, Verderame GM. Experimental Assessment of the Influence of Boundary Conditions on the Out-of-Plane Response of Unreinforced Masonry Infill Walls. *J Earthq Eng* 2018. doi:10.1080/13632469.2018.1453411.
- [31] Walsh K, Dizhur D, Giongo I, Derakhshan H, Ingham J. Predicted Versus Experimental Out-of-plane Force-displacement Behaviour of Unreinforced Masonry Walls. *Structures* 2018;15:292–306. doi:10.1016/j.istruc.2018.07.012.
- [32] Mohebkhah A, Tasnimi AA, Moghadam HA. Nonlinear analysis of masonry-infilled steel frames with openings using discrete element method. *J Constr Steel Res* 2008. doi:10.1016/j.jcsr.2008.01.016.
- [33] Liberatore L, Bruno M, Al Shawa O, Pasca M, Sorrentino L. Finite-discrete element modelling of masonry infill walls subjected to out-of-plane loads. *ECCOMAS Congr. 2016 - Proc. 7th Eur. Congr. Comput. Methods Appl. Sci. Eng., vol. 3, 2016.* doi:10.7712/100016.2175.8924.
- [34] Liberatore L, Marson C, AlShawa O, Pasca M, Sorrentino L. Failure of masonry infill walls under out-of-plane loads. *Proc Int Mason Soc Conf* 2018:78–88.
- [35] Johansen K. *Yield-Line Theory*. Copenhagen: Cement and Concrete Association, London; 1962.
- [36] Johansen K. *Yield-Line Formulae for Slabs*. London: Cement and Concrete Association; 1972.
- [37] Hendry A. The lateral strength of unreinforced brickwork. *Struct Eng* 1973;51:43–50.
- [38] Haseltine B, West H, Tutt J. Design of walls to resist lateral loads. *Struct Eng* 1977;55:422–30.
- [39] Jäger W, Bakeer T. CRITICAL REMARKS ON THE APPLICATION OF THE YIELD LINE METHOD ON MASONRY. 11th Can. Mason. Symp., Toronto, Ontario, May 31- June 3: 2009.
- [40] Drysdale RG, Essawy AS. Out-of-plane bending of concrete block walls. *J Struct Eng* 1988;114:121–33.
- [41] Bakeer T. Theoretical Verification of Existing Solutions on Lateral Loading of Masonry Infill Walls. *Mauerwerk* 2011;15:35–42. doi:10.1002/dama.201100487.
- [42] Griffith M, Vaculik J. Out-of-plane flexural strength of unreinforced clay brick masonry walls. *Mason Soc J* 2007:53–68.
- [43] Hendry AW, Sinha BP, Davies SR. *Design of masonry structures*. London: E & FN Spon; 2004.

- [44] Maluf D, Parsekian G, Shrive N. An Investigation of Out-of-Plane Loaded Unreinforced Masonry Walls Design Criteria. 14th Brick Block Mason Conf 2008:28–37.
- [45] BS 5628-1:2005 Code of practice for the use of masonry. Structural use of unreinforced masonry. London: British Standard Institution; 2005.
- [46] Eurocode 6. Design of Structures for Earthquake Resistance, Part 1: General rules, seismic actions and rules for buildings Masonry Structures, European Committee for Standardization; Brussels, Belgium. 2005.
- [47] S304.1-04 Design of masonry structures. Canadian Standards Association; 2004.
- [48] West HWH, Hodgkinson HR, Haseltine BA. The resistance of brickwork to lateral loading. *Struct Eng* 1977;55:411–21.
- [49] Satti KMH. Model brickwork wall panels under lateral loading. University of Edinburgh, Department of Civil Engineering and Building Science, 1972.
- [50] Hamid AA, Drysdale RG. Flexural Tensile Strength of Concrete Block Masonry. *J Struct Eng* 1988;114:50–66. doi:10.1061/(asce)0733-9445(1988)114:1(50).
- [51] Brown RH, Melander J. Flexural bond strength of masonry parallel to bed joints. 9th Can. Mason. Symp., Frederickson, New Brunswick: 2001.
- [52] Varela-Rivera JL, Navarrete-Macias D, Fernandez-Baqueiro LE, Moreno EI. Out-of-plane behaviour of confined masonry walls. *Eng Struct* 2011;33:1734–41. doi:10.1016/j.engstruct.2011.02.012.
- [53] Varela-Rivera J, Moreno-Herrera J, Lopez-Gutierrez I, Fernandez-Baqueiro L. Out of Plane Strength of Confined Masonry Walls. *J Struct Eng* 2012;138:1331–41. doi:10.1061/(ASCE)ST.1943-541X.0000578.
- [54] Pereira MFP, Pereira MFN, Ferreira JED, Lourenço PB. Behavior of masonry infill panels in RC frames subjected to in plane and out of plane loads. Amcm2011 - 7th Int Conf Anal Model New Concepts Concr Mason Struct 2011.
- [55] Pereira MFP, Pereira MFN, Ferreira JE, Lourenço PB. Infill Masonry : Simple Analytical Methods for Seismic Design. 9th Int Mason Conf 2014:1–12.
- [56] Singhal V, Rai DC. Suitability of Half-Scale Burnt Clay Bricks for Shake Table Tests on Masonry Walls. *J Mater Civ Eng* 2014;26:644–57. doi:10.1061/(asce)mt.1943-5533.0000861.
- [57] Costigan A, Pavia S. Compressive, flexural and bond strength of brick/lime mortar masonry. In: Mazzolani, editor. Proc. PROHITEC 09, Taylor and Francis Group; 2009, p. 1609–15.
- [58] Raposo P, Furtado A, Arêde A, Varum H, Rodrigues H. Mechanical characterization of concrete block used on infill masonry panels. *Int J Struct Integr* 2018;9:281–95.

doi:10.1108/IJSI-05-2017-0030.

- [59] Anić F, Penava D, Varevac D, Sarhosis V. Influence of clay block masonry properties on the out-of-plane behaviour of infilled RC frames. *Teh Vjesn* 2019;26. doi:10.17559/TV-20180222140915.
- [60] Furtado A, Rodrigues H, Arêde A, Varum H. Mechanical properties characterization of different types of masonry infill walls. *Front Struct Civ Eng* 2020. doi:10.1007/s11709-019-0602-y.
- [61] Nalon HG, Santos CFR, Pedroti LG, Ribeiro JCL, Veríssimo G de S, Ferreira FA. Strength and failure mechanisms of masonry prisms under compression, flexure and shear: Components' mechanical properties as design constraints. *J Build Eng* 2020;28:101038. doi:10.1016/j.jobe.2019.101038.
- [62] Singhal V, Rai DC. Role of toothing on in-plane and out-of-plane behavior of confined masonry walls. *J Struct Eng (United States)* 2014;140:1–14. doi:10.1061/(ASCE)ST.1943-541X.0000947.
- [63] Flanagan R, Bennett R. Bidirectional behavior of structural clay tile infilled frames. *J Struct Eng* 1999;125:236–44. doi:10.1061/(ASCE)0733-9445(1999)125:3(236).
- [64] Calvi GM, Bolognini D. Seismic response of reinforced concrete frames infilled with weakly reinforced masonry panels. *J Earthq Eng* 2001;5:153–85. doi:10.1080/13632460109350390.
- [65] da Porto F, Guidi G, Dalla Benetta M, Verlato N. Combined In-Plane/Out-of-Plane Experimental Behaviour of Reinforced and Strengthened Infill Masonry Walls. *12th Can Mason Symp* 2013:1–11.
- [66] Hak S, Morandi P, Magenes G. Out-of-Plane Experimental Response of Strong Masonry Infills. *Second Eur. Conf. Earthq. Eng. Seismol.*, Istanbul: 2014, p. 1–12.
- [67] Morandi P, Hak S, Magenes G. Performance-based interpretation of in-plane cyclic tests on RC frames with strong masonry infills. *Eng Struct* 2018;156:503–21. doi:10.1016/j.engstruct.2017.11.058.
- [68] Furtado A, Rodrigues H, Arêde A, Varum H. Experimental evaluation of out-of-plane capacity of masonry infill walls. *Eng Struct* 2016;111:48–63. doi:10.1016/j.engstruct.2015.12.013.
- [69] Akhoundi F, Vasconcelos G, Lourenço PB, Silva LM. Out-of-plane response of masonry infilled RC frames: Effect of workmanship and opening. *16th Int. Brick Block Mason. Conf.*, 2016, p. 1147–54.
- [70] Wang C. Experimental Investigation on the Out-Of-Plane behaviour of concrete masonry

infilled frame. Dalhousie University Halifax, Nova Scotia, 2017.

- [71] Sepasdar R. Experimental investigation on the out-of-plane behaviour of concrete masonry infilled RC frames. Dalhousie University Halifax, Nova Scotia, 2017.
- [72] Ricci P, Di Domenico M, Verderame GM. Experimental assessment of the in-plane/out-of-plane interaction in unreinforced masonry infill walls. *Eng Struct* 2018. doi:10.1016/j.engstruct.2018.07.033.
- [73] De Risi MT, Di Domenico M, Ricci P, Verderame GM, Manfredi G. Experimental investigation on the influence of the aspect ratio on the in-plane/out-of-plane interaction for masonry infills in RC frames. *Eng Struct* 2019;189:523–40. doi:10.1016/j.engstruct.2019.03.111.
- [74] Di Domenico M, Ricci P, Verderame GM. Experimental assessment of the out-of-plane strength of URM infill walls with different slenderness and boundary conditions. *Bull Earthq Eng* 2019. doi:10.1007/s10518-019-00604-5.
- [75] Akhoundi F, Vasconcelos G, Lourenço P. Experimental Out-Of-Plane Behavior of Brick Masonry Infilled Frames. *Int J Archit Herit* 2020. doi:10.1080/15583058.2018.1529207.
- [76] Morandi P, Hak S, Magenes G. Simplified Out-of-plane Resistance Verification for Slender Clay Masonry Infills in RC Frames. *Proc. 15th Natl. Ital. Conf. Seism. Eng., Padua: 2013.*

Appendix A

Equations of the minimum collapse load, q , for panels of different boundary conditions

In this Appendix equations of the minimum collapse load, q , are obtained by the application of the yield-line method to infill walls taking into account the specific contact conditions that may develop between the masonry and the surrounding frame elements. The collapse load equations are given in general form for three groups: G1 panel supported along four edges; G2 and G3 panel supported along three edges, as shown in Figure A1. Possible collapse mechanisms are shown in Figure A2. Equations of q and β are reported in Table A1. For each boundary condition, the collapse load, q , is the minimum obtained from two different collapse mechanisms (Figure A2).

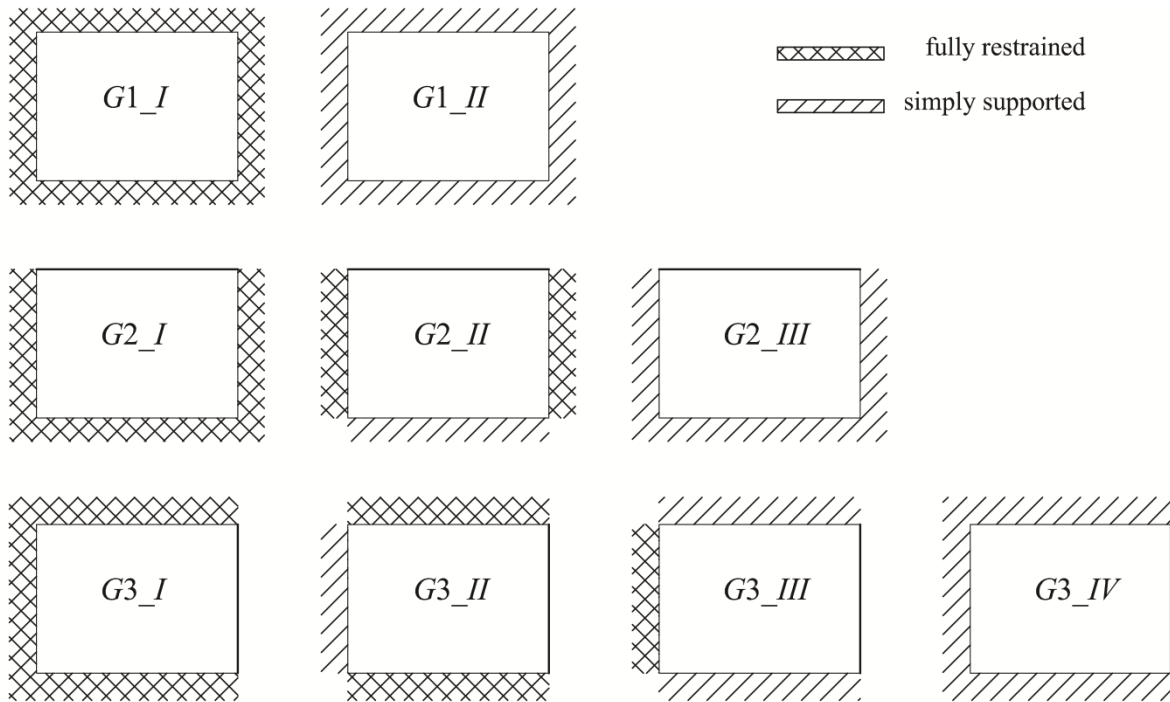


Figure A1: Different boundary conditions: G1 = panel supported along four edges; G2 = panel supported along three edges and free at the top; G3 = panel supported along three edges and free at one vertical edge.

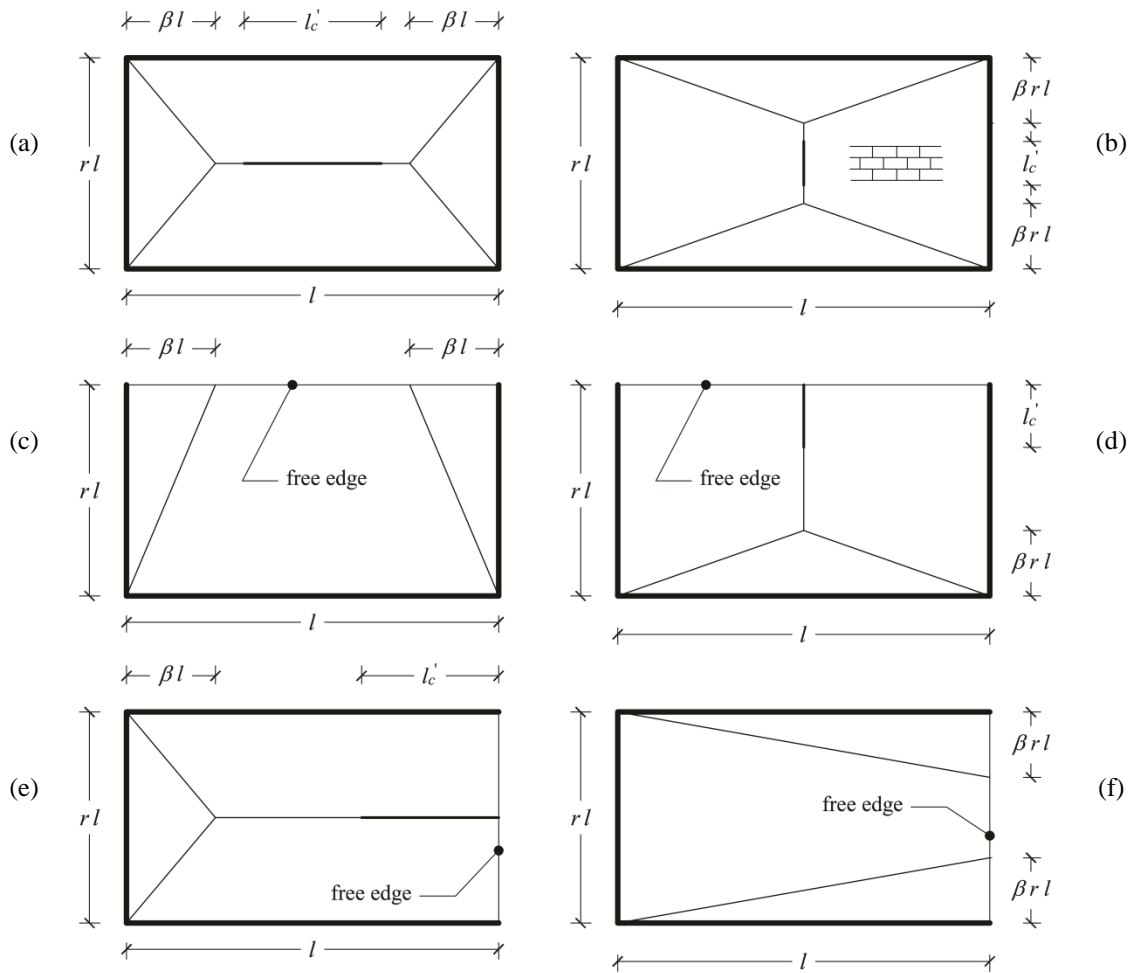

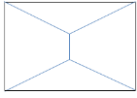



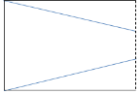


Figure A2: Yield-line patterns, under the assumption of rigid plate rotations about yield-line boundaries: a) and b) possible collapse mechanisms for a panel supported along four edges; c) - d) possible collapse mechanisms for a panel supported along three edges and free at the top; e) and f) possible collapse mechanisms for a panel supported along three edges and free at one vertical edge.

Group and collapse mechanism (Figures A1, A2)	Equations of q and β	
Group G1, mechanism in Figure A2a 	$q = \frac{12m_2(r^2 + 2\beta k\mu + 4\beta^2(1-k)\mu + r^2\gamma_a\mu + 2\beta\gamma_b\mu)}{r^2l^2\beta(3-2\beta)} \quad (A1)$	
	$\beta = \frac{-(1 + \gamma_a)\mu r^2 + r\sqrt{(1 + \gamma_a\mu)(r^2 + 3(3 - 2k)\mu + r^2\gamma_a\mu + 3\gamma_b\mu)}}{2\mu(3 - 2k + \gamma_b)} \leq 0.5 \quad (A2)$	
Group G1, mechanism in Figure A2b 	$q = \frac{12m_2(2r^2\beta k + \mu + 4r^2\beta^2(1-k) + 2r^2\beta\gamma_a\mu + \gamma_b\mu)}{r^2l^2\beta(3-2\beta)} \quad (A3)$	
	$\beta = \frac{-(1 + \gamma_b)\mu + \sqrt{(1 + \gamma_b)(3r^2\mu(3 - 2k) + \mu^2 + 3r^2\gamma_a\mu^2 + \gamma_b\mu^2)}}{2r^2(3 - 2k + \gamma_a\mu)} \leq 0.5 \quad (A4)$	
Group G2, mechanism in Figure A2c 	$q = \frac{6m_2(2r^2 + 2\beta^2\mu + 2r^2\gamma_a\mu + \beta\gamma_b\mu)}{r^2l^2\beta(3-2\beta)} \quad (A5)$	
	$\beta = \frac{-2(1 + \gamma_a\mu)r^2 + r\sqrt{(1 + \gamma_a\mu)(4r^2 + 9\mu + 4r^2\gamma_a\mu + 3\gamma_b\mu)}}{\mu(3 + \gamma_b)} \leq 0.5 \quad (A6)$	
Group G2, mechanism in Figure A2d 	$q = \frac{6m_2(4r^2\beta^2(1-k) + \mu + 4kr^2\beta + 4r^2\beta\gamma_a\mu + \gamma_b\mu)}{r^2l^2\beta(3-\beta)} \quad (A7)$	
	$\beta = \frac{-(1 + \gamma_b)\mu + \sqrt{(1 + \gamma_b)(12r^2\mu(3 - 2k) + \mu^2 + 12r^2\gamma_a\mu^2 + \gamma_b\mu^2)}}{4r^2(3 - 2k + \gamma_a\mu)} \leq 1.0 \quad (A8)$	
Group G3, mechanism in Figure A2e 	$q = \frac{6m_2(r^2 + 4\beta^2\mu + r^2\gamma_a\mu + 4\beta\gamma_b\mu + 4\beta k\mu - 4\beta^2k\mu)}{r^2l^2\beta(3-\beta)} \quad (A9)$	
	$\beta = \frac{-(1 + \gamma_a\mu)r^2 + r\sqrt{(1 + \gamma_a\mu)(r^2 + r^2\gamma_a\mu + 36\mu + 12\gamma_b\mu - 24k\mu)}}{4\mu(3 + \gamma_b - 2k)} \leq 1.0 \quad (A10)$	
Group G3, mechanism in Figure A2f 	$q = \frac{6m_2(2r^2\beta^2 + 2\mu + r^2\beta\gamma_a\mu + 2\gamma_b\mu)}{r^2l^2\beta(3-2\beta)} \quad (A11)$	
	$\beta = \frac{-2(1 + \gamma_b)\mu + \sqrt{(1 + \gamma_b)(4\mu^2 + 4\mu^2\gamma_b + 9r^2\mu + 3\gamma_a r^2\mu^2)}}{r^2(3 + \gamma_a\mu)} \leq 0.5 \quad (A12)$	

q = collapse load; $\mu = f_{x1}/f_{x2}$ = orthogonal ratio, m_2 = yield moment about the vertical direction (Figure 2), r = wall aspect ratio, k = parameter that takes into account the contribution of the first crack to the internal work (for $k = 1$ the first crack is taken into account, for $k = 0$ it is totally disregarded); $\gamma_a = m_a/m_1$ and $\gamma_b = m_b/m_1$, proposed values are reported in Table A2.

Table A1: Equations of q and β .

Wall support condition (Figure A1)	q	γ_a			γ_b			Wall support condition Annex E of [46]
		RC ⁽¹⁾	CM ⁽²⁾	Steel ⁽³⁾	RC ⁽¹⁾	CM ⁽²⁾	Steel ⁽³⁾	
G1_I	\min {Eq. A1, Eq A3}	1	$1/\mu$	0	1	1	0	I
G1_II		0	0	0	0	0	0	E
G2_I	\min {Eq. A5, Eq A7}	1	$1/\mu$	0	1	1	0	D
G2_II		1	$1/\mu$	0	0	0	0	C
G2_III		0	0	0	0	0	0	A
G3_I	\min {Eq. A9, Eq A11}	1	$1/\mu$	0	1	1	0	-
G3_II		0	0	0	1	1	0	-
G3_III		1	$1/\mu$	0	0	0	0	K
G3_IV		0	0	0	0	0	0	J

⁽¹⁾ RC = Reinforced Concrete frame, ⁽²⁾ CM = Confined Masonry, ⁽³⁾ Steel = Steel frame

Table A2: Equations of q , γ_a and γ_b for panels with different boundary conditions.